International Journal of Biological Macromolecules 343 (2026) 150096

Contents lists available at ScienceDirect

International Journal of Biological Macromolecules

journal homepage: www.elsevier.com/locate/ijbiomac

Obesity healthcare via carrageenan-calcium peroxide-generated photothermal micro-polypyrrole carriers☆

Sih-Chi Chuang [a,b,c,g,1], Shih-An Yu [c,1], Pei-Chia Hung [c,1], Cheng-Yi Hsiao [d,e,f,m,1], Lekshmi Rethi [g,h], Hsu-Wei Fang [a], Hieu Trung Nguyen [j], Ke Hung Tsui [k,l,*], Andrew E.-Y. Chuang [g,h,i,**]

[a] Department of Chemical Engineering and Biotechnology, National Taipei University of Technology, Taipei, 10608, Taiwan
[b] Doctoral Program of Biochemical and Biomedical Engineering, National Taipei University of Technology, Taipei, 10608, Taiwan
[c] Hsuan Chen technology CO., LTD. (Taipei Medical University Derived Company), New Taipei City, 22055, Taiwan
[d] Division of Cardiology, Department of Internal Medicine, Taipei Medical University Hospital, Taipei, Taiwan
[e] Cardiovascular Research Center, Taipei Medical University Hospital, Taipei, Taiwan
[f] Division of Cardiology, Department of Internal Medicine, School of Medicine, College of Medicine, Taipei Medical University, Taipei, Taiwan
[g] Graduate Institute of Biomedical Materials and Tissue Engineering, College of Biomedical Engineering, Taipei Medical University, Taipei, 11031, Taiwan
[h] International Ph.D. Program in Biomedical Engineering, College of Biomedical Engineering, Taipei Medical University, Taipei, 11031, Taiwan
[i] Cell Physiology and Molecular Image Research Center, Taipei Medical University-Wan Fang Hospital, Taipei, 11696, Taiwan
[j] Department of Orthopedics and Trauma, Faculty of Medicine, University of Medicine and Pharmacy at Ho Chi Minh city, Ho Chi Minh City, 700000, Viet Nam
[k] Department of Urology, Shuang Ho Hospital, New Taipei City, Taiwan
[l] Department of Medicine, College of Medicine, Taipei Cancer Center, Taipei Medical University, Taipei, Taiwan
[m] Taipei Heart Institute, Taipei Medical University, Taipei, Taiwan

ARTICLE INFO

Keywords:
Obesity healthcare
Carrageenan
Calcium peroxide
Phototherapy
Micro-polypyrrole carrier

ABSTRACT

Obesity is a significant global health challenge, and many existing treatments aimed at reducing appetite or inhibiting fat absorption often have limited success and can cause undesirable side effects. There is a growing need for localized treatment strategies that minimize systemic toxicity while effectively targeting adipose tissue. This study explores the potential of photothermal therapy for obesity treatment using Carrageenan-Calcium Peroxide-generated micro-polypyrrole carriers (PPy-Lec@Car). We aim to assess the efficacy of these carriers in precisely regulating adipose tissue through Near-Infrared (NIR) irradiation, offering an innovative therapeutic platform with potential for non-invasive obesity management. Although injection was used in this preclinical model to ensure targeted delivery, the system is amenable to future non-invasive or minimally invasive clinical applications.

In a preclinical study using a rodent model, PPy-Lec@Car microparticles effectively reduced adipocyte density and fat tissue volume without damaging surrounding healthy tissue, demonstrating a safe and localized treatment effect. A combination of in vitro and in vivo assays, supported by fluorescent imaging, confirmed the photothermal effects of these microparticles on fat cell viability. Mechanistic studies indicated the involvement of Aryl Hydrocarbon Receptor (AhR) activation. Furthermore, 5-ethynyl-2′-deoxyuridine (EdU) proliferation assays revealed a significant reduction in adipocyte viability following PPy-Lec@Car-mediated NIR photothermal stimulation. This study underscores the potential of NIR-activated PPy-Lec@Car microparticles as a promising and localized strategy for safe obesity management.

☆ This article is part of a Special issue entitled: '2025 ISOMRM' published in International Journal of Biological Macromolecules.

* Correspondence to: K.H. Tsui, Department of Urology, Shuang Ho Hospital, New Taipei City, Taiwan.
** Correspondence to: A.E.-Y. Chuang, Graduate Institute of Biomedical Materials and Tissue Engineering, College of Biomedical Engineering, Taipei Medical University, Taipei, 11031, Taiwan.
E-mail addresses: t2130@s.tmu.edu.tw (K.H. Tsui), eychuang@tmu.edu.tw (A.E.-Y. Chuang).

[1] These authors contributed equally.

https://doi.org/10.1016/j.ijbiomac.2026.150096
Received 11 August 2025; Received in revised form 22 December 2025; Accepted 3 January 2026
Available online 5 January 2026
0141-8130/© 2026 Elsevier B.V. All rights are reserved, including those for text and data mining, AI training, and similar technologies.

1. Introduction

Obesity [1–6], characterized by excessive fat accumulation in adipose tissues, often leads to metabolic dysregulation and predisposes individuals to various metabolic disorders, including type 2 diabetes (T2DM), hepatic steatosis, and cardiovascular diseases [7]. Adipose tissue, an endocrine organ with multiple functions, is anatomically and functionally classified into three types: white, brown, and beige fat [8,9]. Beige fat, which is interspersed within white adipose tissue, appears similar to white adipocytes under normal conditions but can undergo a process known as the browning of white fat. This transformation is triggered by cold exposure or beta-adrenergic signaling, leading to the activation of brown fat gene programs and enhanced thermogenesis [10–12].

Clinically, the presence of cold-inducible beige fat in the supraclavicular region of adults holds significant therapeutic potential for treating metabolic diseases [13–15]. Historically, activating beige fat through cold stimuli or adrenergic signaling has been explored as a strategy to combat obesity [11,16]. However, these methods have limited practical applications due to associated health risks, including cardiovascular complications [17–20]. Given the urgency of addressing the obesity epidemic, there is a pressing need to identify new gene targets and develop safe and effective methods for activating beige fat.

Carrageenan (Car) is a high-molecular-weight sulfated polysaccharide commonly used as a food additive, particularly in the meat industry, due to its thickening and gelling properties. As a highly viscous and poorly fermentable soluble dietary fiber, Car has recently gained attention for its potential metabolic benefits. Studies have shown that dietary supplementation with Car can regulate energy metabolism and reduce body weight gain in diet-induced obesity models. Notably, its anti-obesity effects appear to be mediated by the enhancement of energy expenditure rather than reduced caloric intake, primarily through the upregulation of key genes involved in β-oxidation pathways [21,22]. Soy lecithin, a natural phospholipid extracted from soybeans, is a key emulsifier widely used in both food and pharmaceutical industries. Rich in choline, it supports cognitive function, protects liver health, and may help reduce cholesterol levels. Due to its amphiphilic nature, soy lecithin also enhances the stability and bioavailability of compounds, making it valuable in drug delivery and various industrial applications [23–28]. Multiple studies have shown that polypyrrole possesses outstanding photothermal performance and favorable biocompatibility, making it highly promising for various biomedical applications [29–31]. Recent advances in cell-derived nanovesicle (CDN)-based delivery systems for phytochemicals highlight their superior stability, biocompatibility, and encapsulation capacity, offering inspiration for designing our carrageenan-calcium peroxide-based photothermal micro-polypyrrole carriers for obesity management [32].

Photothermal therapy (PTT) offers a promising strategy for localized fat reduction and obesity treatment by using light-induced heat to selectively target adipose tissue. Unlike traditional anti-obesity drugs, which often have limited effectiveness and systemic side effects, PTT can enhance energy expenditure and promote fat metabolism with minimal invasiveness. Recent approaches combine PTT with targeted delivery systems, such as nanoparticles, to improve retention in fat tissue and stimulate beneficial processes like adipocyte browning. This localized, controlled strategy not only reduces fat mass but also helps mitigate obesity-related metabolic complications, providing a safer and more efficient alternative for weight management [33–35].

Recently, hyperthermia therapy (HT), which induces temporary hyperthermia via methods like sauna or hot tub bathing, has gained attention as a potential treatment for metabolic diseases [36,37]. For instance, a study demonstrated that three weeks of daily hot tub bathing led to improved metabolic parameters in T2DM patients, including decreased Hb, mild weight loss, and alleviation of neural-tube defects [38]. Similar metabolic benefits were observed in animal models treated with warm water immersion [39] . These findings support the potential of HT as a therapeutic approach to combat obesity, although it is not yet clear which specific tissues primarily mediate these metabolic benefits. Additionally, prolonged exposure to hot water carries neurological and cardiovascular risks, likely due to elevated core body temperatures and increased production of stress hormones [40]. The role of heat shock protein 72 (HSP72) has been suggested as a mechanism underlying the beneficial effects of HT [41], yet more detailed mechanistic studies are needed. Considering these factors, there is a growing interest in developing localized hyperthermia therapy (LHT) that targets specific tissues such as beige fat, which has demonstrated the capability to autonomously sense temperature changes in a β-adrenergic-receptor-independent manner [42] . This approach aims to minimize the side effects associated with whole-body HT and provide a clearer understanding of the mechanisms involved, thereby enhancing the therapeutic outcomes for individuals battling obesity. However, applying heat therapy to deep tissue for targeted obesity healthcare is essential.

Biomaterials are emerging as revolutionary in various fields, including optoelectronics [43], catalysis [44], and particularly in the biomedical sector [45], where their applications range from biosensing [46] and bioimaging [47] to therapeutic interventions [48]. Within the biomedical realm, non-invasive therapies facilitated by biomaterials, such as hyperthermia [49], photodynamic therapy (PDT) [50,51], photothermal therapy (PTT) [48,52], and radiotherapy [53], are gaining traction. PTT, which uses light to locally induce cell death, combined with strategies that promote the browning of white adipose tissue into heat-producing fat, offers a promising approach for managing obesity [55].

In this study, instead of focusing on traditional disease models, we hypothesize and explore the potential of using photothermal therapy to target and disintegrate fat cells, laying the groundwork for innovative anti-obesity treatments. We utilized the photothermal properties of the core (composed of lecithin (Lec) and calcium peroxide (CaO_2) derived polypyrrole (PPy)) and core-shell microparticles (Carrageenan (Car) coated) as PPy-Lec@Car to treat fat cells under NIR absorption. Subsequent experiments involved evaluating the photothermal effects on fat cell eradication using distinct methods, including cell viability assays, in vitro and in vivo assessments, biochemical fluorescent imaging, and immunofluorescence staining, each employed to investigate the underlying biological mechanisms. To our knowledge, this represents a pioneering proof-of-concept study demonstrating that PPy-Lec@Car can effectively eliminate fat cells in vitro and in vivo, potentially paving the way for future anti-obesity applications using phototherapeutic strategies.

2. Experimental section

2.1. Materials

Various biomaterials and biological tools were procured to facilitate a comprehensive set of biochemical and cellular experiments. Pyrrole monomer (Py), Carrageenan (Car), Lecithin (Lec), 4',6-diamidino-2-phenylindole (DAPI), calcium peroxide (CaO_2), fluorescein isothiocyanate (FITC), and Propidium Iodide (PI) were sourced from Sigma–Aldrich in St. Louis, Missouri, USA. The fat cells were obtained from the Wistar rats, while the cell viability assay kit (Live/Dead kit) was purchased from Thermo Fisher Scientific, USA. Additionally, AhR and RH123 antibodies tagged with fluorescent dyes were acquired from Abscience Co., Ltd., Taipei, Taiwan. These materials are integral to our study, enabling us to perform intricate cellular imaging and viability assays with high reliability and reproducibility.

2.2. Formulation along with characterization

The experimental design included testing various mass ratios of component materials such as Lec, Car, CaO_2, and Py. The ratios tested were 166/6.6/16/16, 166/6.6/16/48, 166/6.6/16/83, 166/6.6/16/

112, and 166/6.6/16/144. These components were mixed at room temperature using a magnetic stirrer set at 100 rpm. The formation and stability of the resultant particles were meticulously analyzed using Dynamic Light Scattering (DLS, Zetasizer Nano ZS instrument, Malvern city, UK) to assess particle size, Polydispersity Index (PDI), and zeta potential.

Furthermore, to fine-tune the material ratios for optimal particle characteristics, FITC fluorescent dye at a concentration of 1 mg/mL was included during the aqueous preparation phase. Morphological changes were observed under a fluorescence microscope (Leica, Germany). The oxidation-reduction potential (ORP) of each sample was measured to determine their oxidative or reductive states, using a spectrometric meter to assess the degree of polymerization. The FTIR analysis was conducted using the Nicolet™ iS™ 10 spectrometers (Thermo Fisher Scientific, MA, USA) to determine the functional groups present in the conjugate and confirm the formation of specific chemical bonds between the components. XRD analysis was performed using a D2 Phaser 2nd Generation X-ray powder diffractometer (Bruker, Massachusetts, USA) to evaluate the crystalline characteristics of the samples. The thermometric analysis was conducted to study photothermal effects of the formulations, respectively. NIR irradiation was performed using an 600–900 nm light diode laser at a power density of 1.5 W/cm^2 for 5 min. The beam spot diameter was approximately 6 mm (0.28 cm^2) at a working distance of 8 cm. During irradiation, local tissue temperatures were monitored to ensure controlled heating. The target temperature range was maintained between 45 and 50 °C, as this range effectively induces apoptosis or necrosis of adipocytes while minimizing injury to surrounding tissues. Care was taken to remain below the thresholds of ~54 °C (immediate lethality) and > 60 °C (coagulative damage), which can adversely affect the epidermis, dermis, or deeper structures. Both irradiation duration and temperature monitoring were controlled, since extended exposures at lower temperatures may yield effects comparable to shorter exposures at higher temperatures [56,57].

2.3. In vitro evaluations

2.3.1. Cytotoxicity and cell viability assessment using rat fat cells

Cytotoxic effects were evaluated using fat cells. The disks, each 10 mm in diameter and 2 mm in height ($n = 3$), were sterilized under UV light for 20 min in a clean bench setting. Cells were seeded at a density of 10^4 cells per well on both sample disks and a tissue culture plate (TCP, used as the control), and incubated at 37 °C in a 5 % CO_2 atmosphere. The growth medium employed was Dulbecco's Modified Eagle Medium (DMEM, Gibco) enriched with 10 % fetal bovine serum (Bioidea) and 1 % streptomycin/penicillin (Gibco).

The MTT assay was used to measure cell proliferation after 24 h of culture by adding MTT solution prepared at 0.5 mg/mL in phosphate-buffered saline (PBS). Formazan crystals formed were solubilized in dimethyl sulfoxide (DMSO, Merck), and the absorbance was read at 490 nm using a microplate reader (Bio-Rad Instruments).

Further, cell viability in contact with the formulated samples was assessed using a Live/Dead assay based on the Calcein AM/ethidium homodimer-1 (EthD-1) kit (Biotium, UK). Following the manufacturer's instructions, cells were treated with the staining solution, incubated at 37 °C for 20 min, washed with PBS, and imaged using an inverted fluorescence microscope (Nikon TE 2000-U, Japan). Cell viability was quantified using ImageJ software by comparing the ratio of live (green) to total cells for each sample set.

To evaluate the cytotoxic effects of the samples under NIR irradiation, cells were seeded and subjected to laser exposure. In preliminary experiments, a range of NIR intensities (1.0–2.0 W/cm^2) and exposure times (0–10 min) were tested to determine suitable conditions that induced measurable effects without causing excessive nonspecific damage. Based on these results, the irradiation parameters were optimized and standardized to 1.5 W/cm^2 for 5 min, which were applied in all subsequent cytotoxicity experiments. The ON-OFF cycles were being done to confirm.

2.3.2. Fluorescent immunostaining for AhR activation and cellular interaction analysis

The impact on the aryl hydrocarbon receptor (AhR) fat cells was analyzed using a combination of fluorescently labeled antibodies as well as nuclei was stained using Propidium Iodide (PI). Afterwards, cells interacting with the formulations were fixed with a 3.7% (*v*/v) paraformaldehyde solution and briefly permeabilized with Triton X-100. Post-washing with PBS, the nuclei were stained with PI solution, and samples were visualized under a fluorescence microscope, allowing precise observation of cellular and subcellular impacts of the formulations. This methodology facilitates a deep understanding of the interactions between the cells and the new biomaterial formulations, highlighting their potential therapeutic benefits.

2.4. In vivo assessments and histological evaluation

All animal procedures were conducted in accordance with protocols approved by the Institutional Animal Care and Use Committee (IACUC No: SHLAC2024-0090 and SHLAC2024-0120) of Taipei Medical University. Male ICR mice (>30 g) were then randomly assigned to four groups: Control, NIR only, PPy-Lec@Car (IP) only, and PPy-Lec@Car (IP + NIR). PPy-Lec@Car was administered intraperitoneally (100 μL/day), and NIR irradiation (600–900 nm, 1.5 W·cm^{-2}, 5 min) was applied every three days over a 14-day period. At the end of the treatment cycle, mice were sacrificed and major organs (heart, liver, spleen, lung, kidney) along with adipose tissues were collected. Tissues were fixed in 10 % formalin, paraffin-embedded, and sectioned into 4 μm slices. Hematoxylin and eosin (H&E) staining was performed to evaluate tissue morphology. Immunohistochemical staining using an antibody against the Aryl hydrocarbon Receptor (AhR) was conducted to assess immune-related responses. Additionally, an EdU (5-ethynyl-2′-deoxyuridine) assay was performed on adipose sections to evaluate cellular proliferation. TUNEL assay was performed on adipose tissue sections using a commercial apoptosis detection kit according to the manufacturer's protocol, with DAPI counterstaining to visualize nuclei and fluorescence microscopy used for imaging. Histological and immunofluorescence images were captured using an optical or fluorescence microscope, and fluorescence intensities were quantitatively analyzed using ImageJ software. These evaluations served as pharmacodynamic indicators to assess therapeutic efficacy and systemic tissue response. Automated analyzers with mouse-specific parameters and algorithms (IDEXX ProCyte Dx and Abaxis VetScan5) were used to perform the blood analysis. On day 14 after therapy, whole blood was obtained by retro-orbital hemorrhage under anesthesia, and the number of red blood cells (RBC), white blood cells (WBC), reticulocytes, platelets, and schistocytes was measured. There were data comparisons between the control and PPy-Lec@Car +NIR.

2.5. Statistical analysis methodology

All data are expressed as mean ± standard deviation (SD). Analyses were conducted using GraphPad Prism v10 (GraphPad Software, USA).

3. Results and discussion

3.1. Exploration of oxygen-crosslinked polymeric formulations

Current research is delving into the potential of polymeric formulations that incorporate oxygen-crosslinked materials as crosslinking agents for enhancing tissue engineering scaffolds. These materials are characterized by their adjustable viscoelastic properties, biocompatibility, and controlled degradation rates. In this investigation, pyrrole (Py) underwent oxidative polymerization in a solution containing calcium peroxide (CaO_2) and a lecithin analog derived from soybean oil

(LEC). This process resulted in the generation of ionomeric composites with varied chemical structures tailored to meet the mechanical and biological properties of native tissues. Oxygen-releasing biomedical materials used as crosslinking agents enhance the polymers' biocompatibility and bioactivity, facilitating cell attachment and proliferation. Furthermore, the biodegradability of these composites is crucial as it enables their degradation to be synchronized with natural tissue regeneration processes.

3.2. Optimization of formulation

Size distribution analysis of Lec/Car/CaO_2/Py composites revealed that particle size changed with increasing Py content. At a ratio of 166/6.6/16/16, particles were ~ 7800 nm, while increasing Py to 48 and 83 reduced sizes to about 5000 nm and 2000 nm, respectively indicating improved particle formation. However, further increases to 112 and 144 led to fluctuations (4100 nm and 8000 nm), suggesting instability at higher ratios. These results highlight the importance of precise component balancing to achieve optimal particle characteristics for biomedical applications (Fig. 1a).

The Poly Dispersity Index (PDI) analysis of Lec/Car/CaO_2/Py composites (Fig. 1b) highlighted the impact of component ratios on particle uniformity. At 166/6.6/16/16, a high PDI of about 1.0 indicated broad size distribution. Increasing Py to 48 and 83 reduced the PDI to 0.3 and 0.2, respectively, reflecting greater uniformity. However, further increases to 112 and 144 caused fluctuations, with PDI values rising to 0.6 and 0.65. These results emphasize the importance of optimized formulation to achieve consistent particle size and stability in biomedical

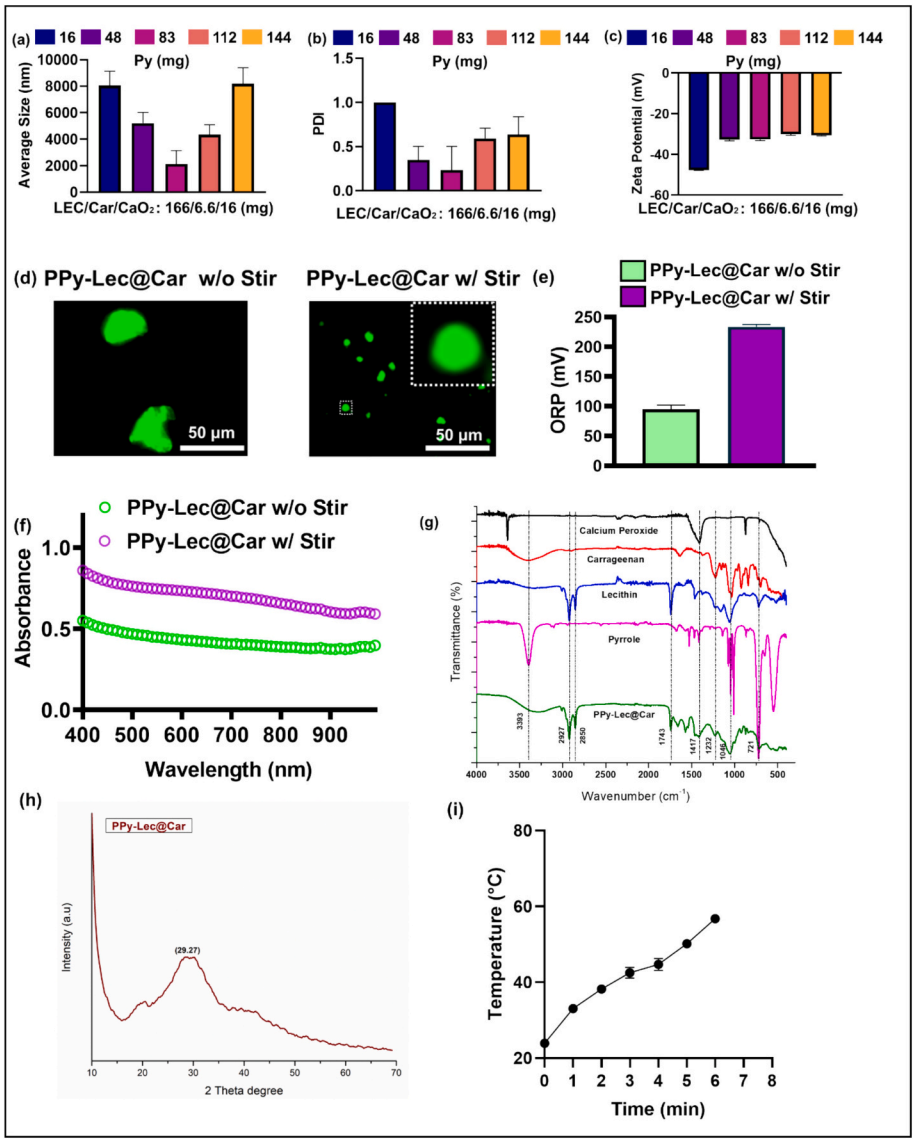

Fig. 1. Characterization of PPy-Lec@Car Microparticles. (a) Particle Size Distribution: Graph showing size reduction from ~8,000 nm to 2000 nm with increased Py concentration (16 mg to 83 mg), then increase to 9000 nm at 144 mg Py. (b) Polydispersity Index (PDI) Data indicating optimal formulation (166/6.6/16/83) with a PDI below 0.5, suggesting good uniformity. (c) Zeta Potential Measurement: Graph showing a negative charge of ~ − 30 mV for the optimal formulation, highlighting the stabilizing role of the Car polymer. Analysis of PPy-Lec@Car Microparticles Under Different Mixing Conditions. (d) Fluorescence microscopy shows uniform particle distribution with magnetic stirring, compared to aggregation without stirring. (e) ORP measurements indicate higher oxidation (above 200 mV) in stirred samples, reflecting more effective polymerization. (f) Spectrometric absorbance data from 400 to 900 nm shows higher absorbance in stirred samples, suggesting successful PPy formation and suitability for NIR photothermal applications. (g) FTIR analysis reveals characteristic peaks for the composite's functional groups. (h) XRD shows an amorphous pattern with no distinct peaks. (i) PTT evaluation demonstrates efficient photothermal conversion, with a gradual temperature increase under NIR irradiation, highlighting the composite's potential for photothermal therapy.

applications (Fig. 1b). According to previous studies, a PDI value under 0.5 is generally considered acceptable for pharmaceutical and biomedical applications, reflecting good stability and homogeneity of the particles. For instance, nanoparticle suspensions for drug delivery have been reported to exhibit satisfactory performance when maintaining a PDI below 0.5, supporting the suitability of our micro particles for further in vivo application [58].

Zeta potential analysis of Lec/Car/CaO_2/Py composites (Fig. 1c) revealed that the 166/6.6/16/16 ratio had the highest negative charge at −42 mV, indicating excellent colloidal stability. Other ratios 166/6.6/16/48, 83, 112, and 144 showed slightly changed values of −30, −30, −28, and − 29 mV, respectively, still reflecting good stability. These variations demonstrate the effect of component ratios on surface charge and highlight the need for precise formulation to ensure optimal stability for biomedical use (Fig. 1c).

The polymerization of Py is influenced by oxygen-releasing agents like LEC and CaO_2, which help form a LEC-PPy complex encapsulated by the Car polymer, resulting in a core-shell structure. Dynamic Light Scattering (DLS) data showed that the smallest particle size and best stability were achieved at a formulation ratio of 166/6.6/16/83 [59,60]. This formulation was chosen for further experimentation due to its low polydispersity index (PDI) below 0.5 and a negative zeta potential of approximately −30 mV, indicative of the Car acting as a stabilizing shell.

The oxidative polymerization capabilities of Py with other monomers such as thiophene, and aniline have been well-documented [61]. CaO_2 acts as a crucial oxidizing agent, facilitating the release of oxygen during its reaction with water, which is beneficial for various applications including environmental remediation and medical treatments as an oxygen supplier [62]. Carrageenan (Car), the chosen anionic polymer, is particularly notable for its structure of alternating units of hemisulfated galactose and 3–6 anhydrogalactose, making it highly effective in forming stable, anionically charged microparticles [63].

3.3. Microscopic and spectrometric characterization

Fluorescence microscopy (Fig. 1d) showed that magnetic stirring during formulation produced uniformly distributed PPy-Lec@Car microparticles (PPy-Lec@Car w/Stir) with excellent colloidal stability, while unstirred samples (PPy-Lec@Car w/o Stir) formed large, aggregated particles. Stirring effectively promoted dispersion and homogeneity, emphasizing its critical role in achieving optimal particle characteristics for biomedical applications [64,65]. ORP measurements (Fig. 1e) showed that stirred PPy-Lec@Car composites had higher oxidation levels (>200 mV) compared to non-stirred samples (~100 mV), indicating enhanced oxidative polymerization [66,67]. This highlights the role of stirring in promoting chemical interactions and improving composite properties through better dispersion and reactivity. Spectrometric analysis (Fig. 1f) showed higher absorbance in stirred PPy-Lec@Car formulations, indicating more effective PPy formation and improved NIR photothermal conversion [68]. This highlights the significance of stirring in enhancing the composite's optical properties for photothermal therapy applications.

FTIR analysis (Fig. 1g) of the individual components and the composite PPy-Lec@Car revealed key functional groups. Calcium peroxide showed peaks at 3642 cm^{-1} (O—H stretch) and 865 cm^{-1} (peroxide) [69,89]. Carrageenan exhibited peaks at 3393 cm^{-1} (O—H), 1241 cm^{-1} (O=S=O), 925 cm^{-1} (ether group), and 848 cm^{-1} (C_4-O-S) [70]. Lecithin displayed peaks at 2921 cm^{-1} (CH_2 stretch), 2848 cm^{-1} (CH_2 stretch), 1744 cm^{-1} (C=O), 1466 cm^{-1} (CH_2 bend), and 1057 cm^{-1} (C—C) [71]. Pyrrole had peaks at 3391 cm^{-1} (N—H) and 726 cm^{-1} (C—H bend) [72]. In the PPy-Lec@Car microparticles, key peaks included 3393 cm^{-1}, 2927 cm^{-1}, 2850 cm^{-1} (C—H), 1743 cm^{-1} (C=O), 1417 cm^{-1} (CH_2 bend), and 1232 cm^{-1} (C—O),1046 (C—O stretch),721 (C—H bend) indicating successful integration of components and molecular interactions. The observed shifts in the FTIR absorption bands indicate successful particle formation through chemical interactions among the constituent components. X-ray diffraction (XRD) analysis of the PPy-Lec@Car microparticles revealed a peak at 29.27°, indicating its amorphous nature, with no distinct diffraction peaks (Fig. 1h). This suggests a disordered atomic structure. The photothermal evaluation showed a gradual temperature increase from 25 °C at 0 min to 57 °C at 6 min (Fig. 1i), demonstrating the composite's efficient light-to-heat conversion, making it suitable for photothermal applications like targeted therapy and drug release.

The photo thermal stability of PPy-Lec@Car nanoparticles was evaluated under repeated near-infrared (NIR) on/off irradiation cycles. Starting from a baseline temperature of 25 °C, irradiation for 5 min elevated the suspension temperature to 58.0 °C during the first cycle. After the NIR source was switched off, the temperature decreased to about 37 °C. A second heating cycle reached 57.9 °C before cooling to 37.3 °C, while a third cycle peaked at 57.1 °C and cooled to about 37 °C. Across the three cycles, the maximum temperature decreased by less than 1 °C (58.0 to 57.1 °C), demonstrating excellent reproducibility and thermal stability of PPy-Lec@Car under repeated photo thermal activation. These findings confirm the robustness of the nanoparticles in sustaining consistent heat generation during NIR irradiation, which is critical for reliable therapeutic performance in photo thermal applications (Fig. S1).

3.4. Biological assays and fat cellular responses

Fat cells are sensitive to hyperthermia, leading them to undergo damage [56]. Cell viability and count are critical metrics in diverse research areas, from assessing metabolic activities [73] to normalizing data in Western blot analyses [74]. Typically, cell viability and number are quantified using fluorescence-based live/dead assays. Such assays commonly employ dyes like calcein-acetoxymethyl ester (calcein-AM) and ethidium homodimer-1 or propidium iodide (PI), (Invitrogen, Carlsbad, CA, USA) [75]. Calcein-AM itself is not inherently fluorescent but becomes permeable to cell membranes. Once inside live cells, cellular esterases cleave calcein-AM to release calcein, which fluoresces bright green.

The MTT assay assesses cell viability by measuring mitochondrial activity, where living cells convert MTT into formazan crystals. Biological assays, including MTT and Live/Dead, showed that PPy-Lec@Car microparticles (PPy-Lec@Car w/o NIR) at 0.28 mg/mL significantly reduced cell viability when activated by NIR therapy (PPy-Lec@Car w/NIR), compared to higher concentrations (0.55, 1.1, 2.2, and 4.4 mg/mL) with and without NIR exposure (Fig. 2a-b). At 0.28 mg/mL, viability increased to 144 % without NIR, but dropped to 15.90 % with NIR. At 0.55 mg/mL and 1.1 mg/mL, viability was 173.4 % and 144.3 % without NIR, and 14.6 % and 15.96 % with NIR. At higher concentrations (2.2 mg/mL and 4.4 mg/mL), viability without NIR was 115.3 % and 51.35 %, while NIR exposure led to 20.8 % and 24.20 % viability, respectively. These findings indicate a concentration-dependent effect of PPy-Lec@Car on cell viability, modulated by NIR-induced photothermal effects (Fig. 2a). Live/Dead assay results (Fig. 2b) supported the MTT findings, showing the control group with more live cells and fewer dead cells. NIR exposure increased live cell counts and reduced dead cells compared to the control. PPy-Lec@Car without NIR showed similar live cell counts to the control, indicating biocompatibility. However, with NIR exposure, live cell counts decreased and dead cells increased, suggesting a photothermal effect induced by the composite.

The micrometer-scale size of the particles facilitates their retention within the loose extracellular matrix of fat tissue following intraperitoneal injection, allowing for localized interaction with adipocytes. This passive accumulation is critical for achieving effective photothermal therapy while minimizing systemic distribution. Prior work with drug-loaded PLG microparticles, such as resveratrol formulations, has shown that particle surface characteristics and drug distribution can significantly influence tissue interaction and therapeutic outcomes. Similarly, our optimized PPy-Lec@Car microparticles exhibited good

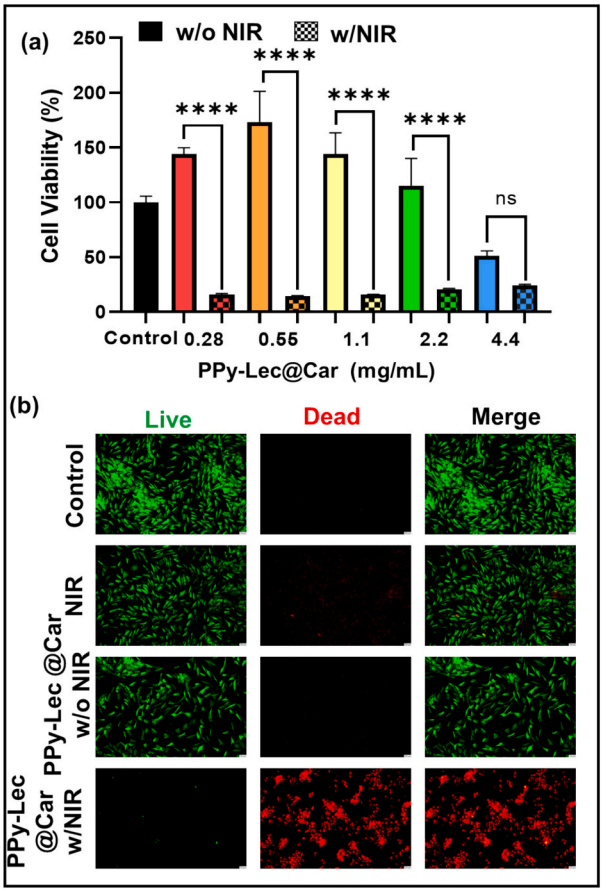

Fig. 2. Cell viability and proliferation analysis with PPy-Lec@Car microparticles under NIR treatment. (a) MTT assay results: Illustrates the reduction in cell viability at a concentration of 0.28 mg/mL of PPy-Lec@Car when combined with NIR therapy, compared to higher concentrations (0.55, 1.1, 2.2, and 4.4 mg/mL), both with and without NIR exposure. The data depicts lower cell viability at optimal concentrations, indicating the effectiveness of targeted NIR activation. (b) Live/dead assay results: Shows fluorescence microscopy images that provide visual evidence of cell viability, with reduced viability observed at 0.28 mg/mL concentration when activated by NIR.

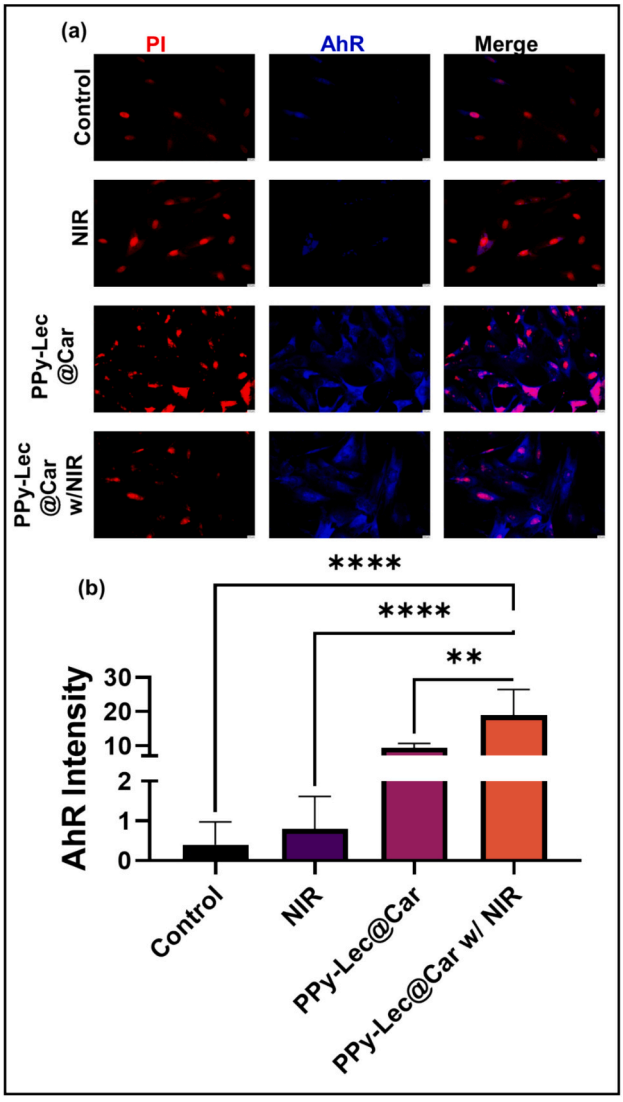

Fig. 3. Aryl hydrocarbon receptor (AhR) expression in cells treated with PPy-Lec@Car microparticles. (a) qualitative and (b) quantitative data. This figure presents fluorescence microscopy images demonstrating significant AhR expression in cells exposed to PPy-Lec@Car microparticles under NIR treatment. The data highlight the active engagement of AhR, which might be critical for responding to environmental polycyclic aromatic hydrocarbons (PAHs), validating the biochemical mechanism through which the microparticles exert their effects. This activity supports the potential of PPy-Lec@Car in targeted regenerative and molecular therapies by modulating cellular responses to external stimuli.

colloidal stability, appropriate size, and photothermal properties, which enabled selective disruption of adipose tissue upon NIR irradiation. The observed adipose tissue damage and reduced cellular proliferation, along with minimal off-target effects in other organs, further support that appropriately engineered microparticles can serve as an effective platform for localized fat-targeted therapies. These findings highlight the importance of controlling particle size, surface properties, and localized activation to maximize therapeutic efficacy against obesity [76].

The AhR is a transcription factor that is traditionally recognized for its role in mediating the toxic effects of dioxins and other environmental pollutants. However, recent studies have revealed that AhR also plays a broader role in various biological processes, including cell cycle regulation, immune response modulation, and apoptosis (programmed cell death) [77,78]. AhR can induce apoptosis in certain cell types upon activation by specific ligands. This is often mediated through the transcriptional activation of genes associated with the apoptotic pathway. Overall, AhR's involvement in cell death is complex and can vary greatly depending on external and internal factors influencing the cell [79,80].

Fluorescence microscopy (Fig. 3a) showed significant Aryl Hydrocarbon Receptor (AhR) expression in cells treated with PPy-Lec@Car microparticles, aligning with previous studies on AhR's response to aromatic structures [81]. The AhR staining assay revealed low expression in the control group, a reduction in the NIR group, and a slight increase in the PPy-Lec@Car group. However, with NIR exposure, the PPy-Lec@Car microparticles showed a significant increase in AhR expression, suggesting activation by NIR. Quantitative analysis (Fig. 3b) showed baseline AhR intensity of 0.2 in the control, 0.5 in the NIR group, and a high intensity of 10 in the PPy-Lec@Car group, which increased to 18 upon NIR exposure. These findings highlight the potential of PPy-Lec@Car in modulating AhR expression for therapeutic applications, warranting further investigation into the underlying mechanisms. Similar to the RGD/CS/β-GP hydrogel, which demonstrated biocompatibility, controlled degradation, and enhanced wound healing [82] our PPy-Lec@Car system also exemplifies how rationally engineered biomaterials can address specific therapeutic challenges. While the hydrogel provides advanced solutions for wound management, the PPy-Lec@Car platform applies NIR-driven photothermal

activation to selectively target adipose tissue, inducing apoptosis and metabolic regulation without organ toxicity.

3.5. Animal examinations of phototherapeutic PPy-Lec@Car microparticles

According to the animal experiments (Fig. 4), PPy-Lec@Car microparticles were delivered via intraperitoneal (IP) injection into the mice. The temperature elevation experiments (Fig. 4a) indicated that, following NIR irradiation, the group treated with IP injection of PPy-Lec@Car microparticles experienced an increase in localized tissue temperature to mild hyperthermia levels. This temperature rise was recorded and significantly higher compared to both the untreated control group and the group that received PPy-Lec@Car microparticles without NIR exposure.

Histopathological analysis using hematoxylin and eosin (H&E) staining (Fig. 4b) revealed no significant differences in the heart, liver, spleen, lung, and kidney tissues across all experimental groups, including the untreated control group, the NIR-only group, the PPy-Lec@Car microparticle IP injection group, and the combined PPy-Lec@Car microparticle IP injection + NIR group. These findings suggest that the combination of PPy-Lec@Car microparticles and NIR does not induce noticeable damage to major internal organs, supporting the biocompatibility and safety of this treatment. Fig. 4b shows that in some areas of the adipose tissue section, there is no obvious adipocyte structure, and only a small amount of interstitial and connective tissue remains. This phenomenon may not be simply due to lipid loss caused by paraffin embedding, but rather reflects that the materials used in this

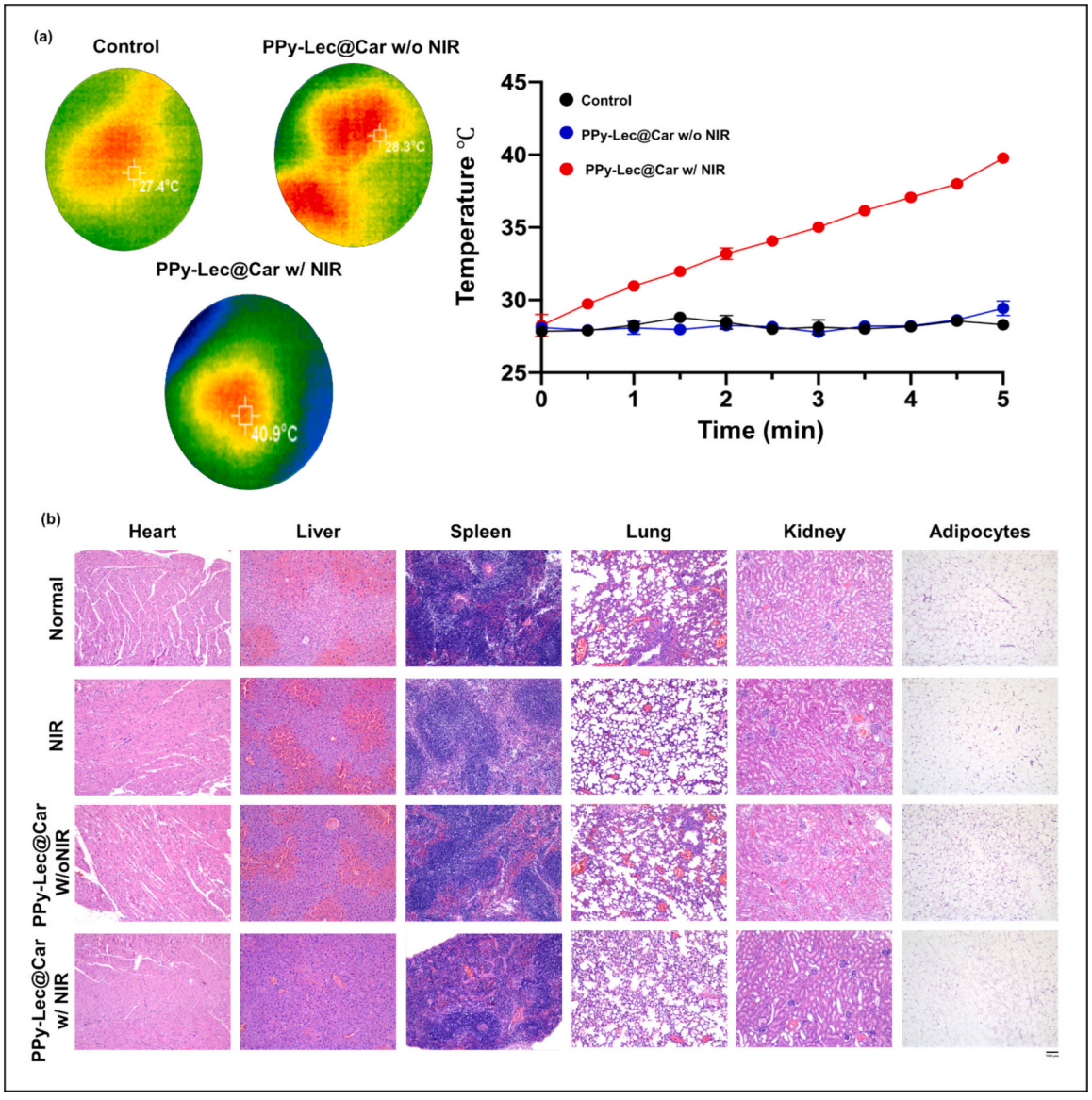

Fig. 4. Intraperitoneal (IP) injection of PPy-Lec@Car microparticles into mice, followed by NIR irradiation. (a) The temperature elevation results show that the combination of IP injection of PPy-Lec@Car microparticles and NIR irradiation leads to a significant increase in tissue temperature to mild hyperthermia levels compared to both the untreated control group and the PPy-Lec@Car microparticle IP injection group without NIR (Temperature mapping experiments were performed individually on all mice. The image shown here is a representative result). (b) Hematoxylin and eosin (H&E) stained histopathological sections of various organs (heart, liver, spleen, lung, kidney and adipocytes/tissue) from different experimental groups, including untreated control, NIR-only, PPy-Lec@Car microparticle IP injection, and PPy-Lec@Car microparticle IP injection + NIR. Histological analysis showed no clear evidence of organ damage, confirming the treatment's biocompatibility. In adipose tissue, the untreated control, NIR-only, and PPy-Lec@Car microparticle IP injection groups maintained an intact reticular structure. However, the PPy-Lec@Car microparticle IP injection + NIR group displayed disrupted and irregular adipose morphology, suggesting effective induction of adipose tissue apoptosis and damage. These results highlight the potential of this treatment approach for targeted fat reduction.

experiment promote the reduction of adipose tissue. Since adipocytes are mainly composed of lipids, when the material promotes lipolysis or adipocyte apoptosis, the lipid content in the tissue decreases significantly, further leading to the collapse of the tissue structure. After HE staining, it shows a partial cell loss and loose structure, supporting the potential delipidation effect of the material.

Interestingly, in the analysis of adipose tissue, distinct differences were observed between the experimental groups. In the untreated control group, the NIR-only group, and the PPy-Lec@Car microparticle IP injection group, the adipose tissue maintained an intact and organized reticular structure. However, in the group treated with both PPy-Lec@Car microparticles and NIR, the adipose tissue displayed irregular morphology, with a disruption of the reticular fat structure. This observation suggests that the combination of PPy-Lec@Car microparticles and NIR may effectively induce apoptosis or damage to adipose tissue.

At 14 days post-treatment, hematological analysis showed that red blood cell (RBC) and platelet counts were nearly identical between the control group (8.6 M/μL RBC, 961 K/μL platelets) and the PPy-Lec@Car w/ NIR group (8.61 M/μL RBC, 962 K/μL platelets), indicating no significant hematological disturbance. Reticulocyte counts were slightly lower in the PPy-Lec@Car w/ NIR group (256.6 K/μL) compared to

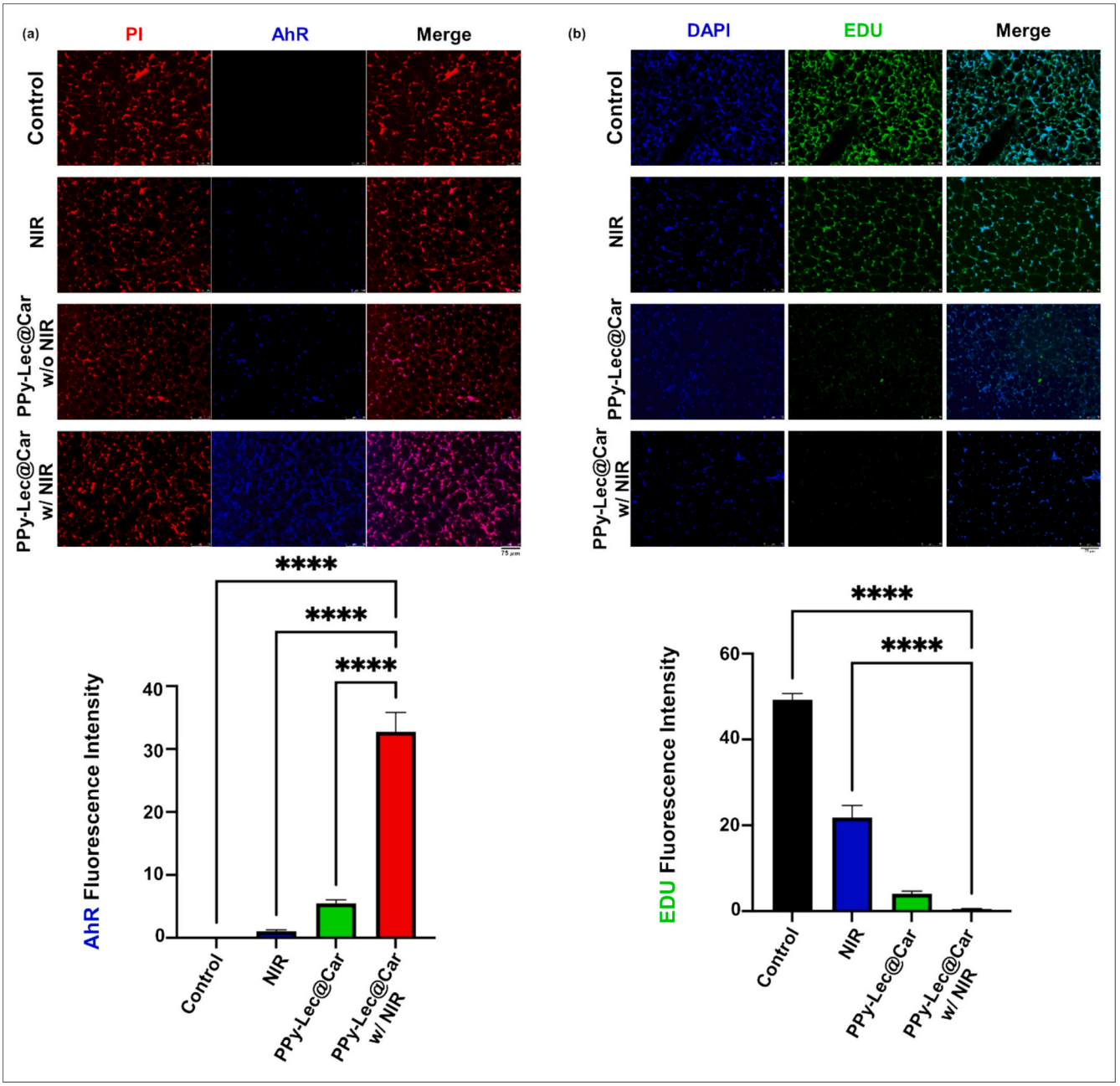

Fig. 5. Fluorescence microscopy analysis of adipose tissue from different experimental groups: untreated control, NIR-only, PPy-Lec@Car microparticle IP injection, and PPy-Lec@Car microparticle IP injection + NIR. (a) The group treated with PPy-Lec@Car microparticles w/NIR exhibited the highest expression of Aryl hydrocarbon Receptor (AhR) in adipose tissue, suggesting enhanced activation of stress-related pathways, compared to the other groups. (b) Additionally, this group showed the lowest levels of 5-Ethynyl-2′-deoxyuridine (EDU) incorporation, indicating reduced cellular proliferation in adipose tissue, likely due to the induction of cellular stress and apoptosis. The combination of increased AhR expression and decreased EDU levels supports the hypothesis that the PPy-Lec@Car microparticles w/NIR treatment effectively targets adipose tissue, promoting selective damage and inhibiting fat cell regeneration. These results highlight the potential of this approach for targeted adipose tissue reduction.

control (319 K/μL), while white blood cell (WBC) counts were mildly elevated (4.25 K/μL vs. 3.14 K/μL), possibly reflecting a minimal immune response. Overall, the data suggest that the hematological profiles of both groups remain largely comparable, with only minor differences that may not indicate any substantial physiological disruption due to the treatment (Fig. S2).

These results imply that the photothermal properties of PPy-Lec@Car microparticles, when combined with NIR irradiation, can specifically target and disrupt adipose tissue. This mechanism could offer a promising strategy for treating obesity or reducing unwanted fat deposits in a safe and controlled manner. The selective damage to adipose tissue without affecting other vital organs highlights the potential of this approach for localized fat reduction therapies, potentially offering a non-invasive alternative to traditional fat removal techniques. Targeted modulation of biological pathways has been demonstrated in recent work where a metal-based Ir(III) complex disrupted EED–EZH2 interactions, suppressing cancer progression through epigenetic regulation [83]. In parallel, our PPy-Lec@Car system applies NIR-driven photothermal activation to selectively modulate adipose tissue, achieving localized apoptosis and metabolic regulation without organ toxicity. Both strategies highlight the promise of rationally designed therapeutic platforms for safe and effective disease management.

Future investigations should focus on further optimizing the NIR exposure parameters and exploring the long-term effects of this treatment. Additionally, the molecular mechanisms underlying the selective adipose tissue apoptosis observed in this study warrant further exploration. Understanding how PPy-Lec@Car microparticles and NIR induce fat cell death could provide valuable insights into developing targeted therapies for metabolic disorders and obesity-related conditions.

To gain deeper insights into the underlying mechanisms of the in vivo animal experiments, fluorescence microscopy was employed to assess the effects on adipose tissue across different experimental groups: untreated control, NIR-only, PPy-Lec@Car microparticle IP injection, and the combination of PPy-Lec@Car microparticles IP injection with NIR irradiation.

As shown in Fig. 5a, the group treated with both PPy-Lec@Car microparticles and NIR demonstrated the highest expression of Aryl hydrocarbon Receptor (AhR) in adipose tissue compared to the other groups (untreated control, NIR-only, and PPy-Lec@Car microparticle IP injection without NIR). This elevated AhR expression suggests a possible activation of cellular stress responses or metabolic pathways related to lipid metabolism, which may be triggered by the combined photothermal and microparticle treatment. AhR is known to play a role in modulating various biological processes, including inflammation and oxidative stress, which could be contributing to the observed tissue responses.

In this study, EDU staining (Fig. 5b) was employed to evaluate cell proliferation in adipose tissue, as EDU incorporation indicates active DNA synthesis during cell division. The control group and NIR-only group exhibited relatively higher levels of EDU staining, reflecting normal adipocyte proliferation. Similarly, the PPy-Lec@Car microparticle group without NIR exposure showed no significant change in EDU expression compared to the control, confirming the biocompatibility of the microparticles in the absence of photothermal activation. In contrast, the PPy-Lec@Car + NIR group demonstrated a marked reduction in EDU staining, suggesting that NIR-activated photothermal treatment significantly suppressed adipocyte proliferation. This decrease in EDU incorporation indicates that the combined treatment induced cellular stress or apoptosis, impairing the regenerative capacity of adipose tissue. Together with the observed AhR upregulation and histological disruptions, these findings further support the effectiveness of the PPy-Lec@Car microparticles under NIR irradiation in selectively targeting and inhibiting fat tissue growth [84].

The combination of increased AhR expression and decreased EDU levels provides further evidence of the dual effect of this treatment promoting stress responses while inhibiting cell growth potentially leading to adipocyte apoptosis or dysfunction. This suggests that PPy-Lec@Car microparticles, when activated by NIR, could serve as a novel approach for targeted fat reduction, particularly in the context of obesity or unwanted fat deposits. By inducing selective damage to adipose tissue, this strategy offers a non-invasive alternative to traditional fat removal methods. Future research should aim to clarify the molecular pathways by which AhR is activated in adipose tissue in response to this treatment and further explore the long-term effects of reduced cellular proliferation on fat tissue dynamics. Additionally, understanding the broader implications of AhR activation in relation to metabolic regulation and tissue homeostasis could provide valuable insights into the therapeutic potential of this approach. Our findings suggest that PPy-Lec@Car + NIR treatment may reduce EdU staining partly through AhR activation, although this mechanism requires further validation. In future studies, we plan to investigate this pathway more directly by incorporating AhR antagonists, knockdown strategies, and quantification of downstream targets, which will help to clarify the relative contributions of photothermal cytotoxicity versus AhR-dependent signaling.

NIR photothermal therapy has been shown to reduce body weight and fat mass by targeting adipose tissue through multiple mechanisms. The therapy induces the transformation of white adipose tissue into metabolically active brown or beige fat, thereby increasing energy expenditure, as highlighted by the previous studies [86,87]. When delivered via nanoparticles that absorb NIR light, localized heating damages fat cells, leading to lipolysis and apoptosis [88]. This targeted reduction in both subcutaneous and visceral adipose tissue addresses major sites of fat accumulation in obesity. Evidence from rodent studies demonstrates significant decreases in adipose tissue mass, improvements in metabolic profiles such as reduced serum cholesterol and inflammation, and in some cases, concurrent increases in lean mass, together indicating an overall improvement in body composition [35,86–88].

TUNEL assay (Fig. 6a) was performed to evaluate apoptosis in adipose tissue under various treatment conditions. In the control group, no TUNEL-positive signal was observed, indicating an absence of apoptosis. The NIR-only group showed a slight increase in TUNEL signal, suggesting minor induction of apoptotic activity due to NIR irradiation. In the group treated with PPY-Lec@Car alone, a low level of TUNEL-positive staining was detected, indicating limited apoptotic effect of the nanomaterial without photothermal activation. In contrast, the PPY-Lec@Car + NIR group exhibited a substantial increase in TUNEL-positive cells, confirming a strong apoptotic response. These results demonstrate that PPY-Lec@Car nanocomposite alone or NIR alone induces only minimal apoptosis in adipose cells. However, the combination of PPY-Lec@Car with NIR irradiation significantly enhances apoptotic activity, as evidenced by strong TUNEL staining. This suggests that the photothermal effect of PPY-Lec@Car under NIR exposure plays a critical role in initiating cell death pathways. The synergistic effect highlights the potential of PPY-Lec@Car as an effective agent for NIR-triggered apoptosis induction, possibly through localized hyperthermia and disruption of cellular homeostasis in adipose tissues. Body weight (Fig. 6b) was monitored over a 14-day period to evaluate the systemic impact of treatments. The control group exhibited steady weight gain throughout the study, indicating normal physiological status. Similarly, the PPy-Lec@Car group showed a gradual increase in body weight, with values nearly matching those of the control group by Day 14, suggesting good biocompatibility and no adverse effects from the microparticles alone. In contrast, the PPy-Lec@Car + NIR group displayed a progressive decline in body weight, with a significant reduction observed by Day 14. This downward trend may be attributed to localized hyperthermia-induced fat reduction or systemic metabolic effects following photothermal therapy. These findings support the potential of PPy-Lec@Car + NIR as an effective strategy for targeted fat reduction while emphasizing the need to monitor systemic effects during prolonged treatment.

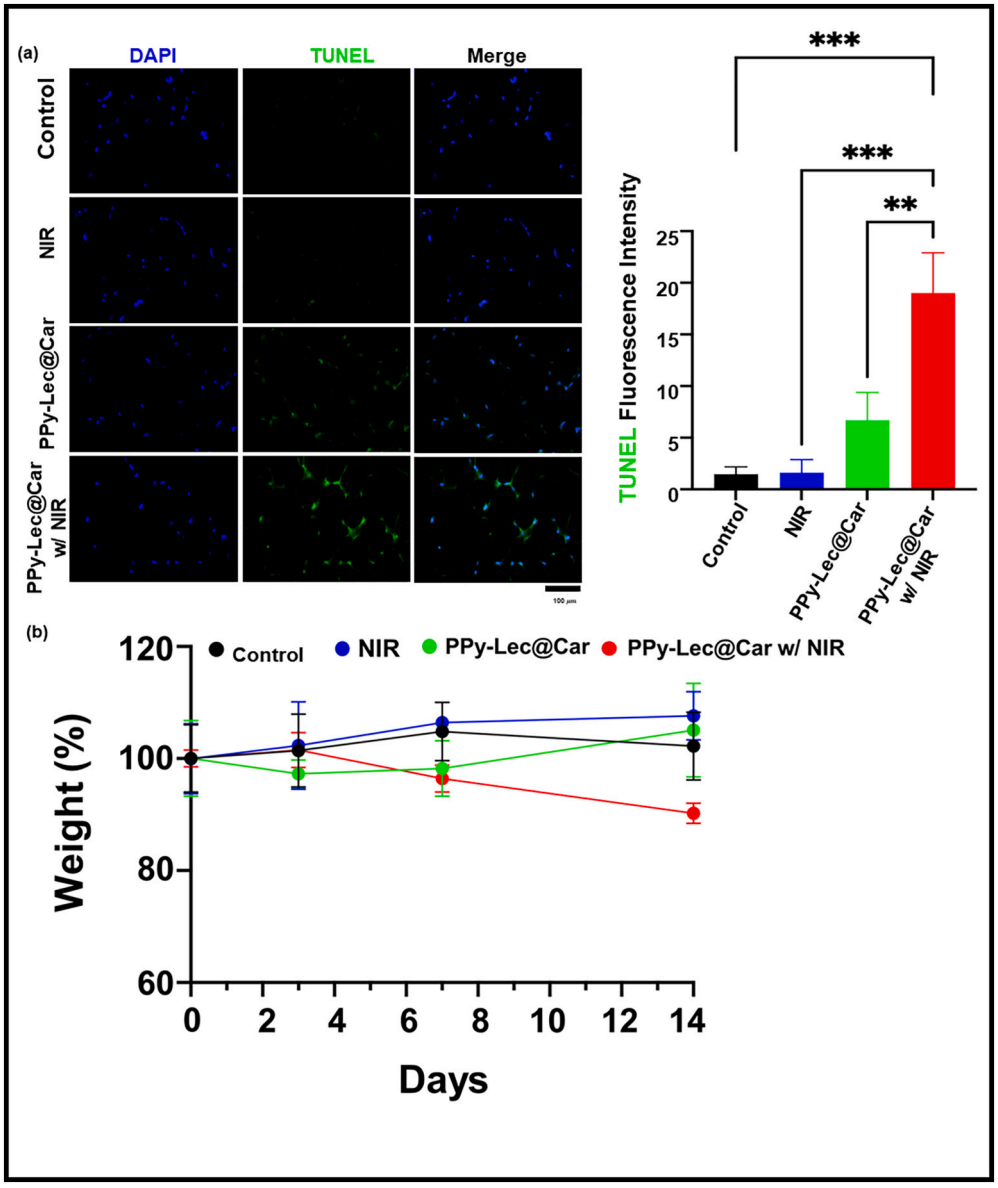

Fig. 6. (a) Representative fluorescence images showing TUNEL-positive apoptotic cells in untreated control group (no signal), NIR-only group (weak signal), PPY-Lec@Car-treated group (low signal), and PPY-Lec@Car + NIR group (strong TUNEL signal indicating extensive apoptosis). Nuclei were counterstained with DAPI (blue), and TUNEL-positive cells appear green. The marked increase in TUNEL signal in the PPY-Lec@Car + NIR group confirms that NIR-induced photothermal activation significantly enhances apoptotic cell death in adipose tissue. The quantitative data is also included. (b) Weight changes of the animal treated with different groups.

4. Conclusion

This study demonstrates the development of PPy-based suspension microparticles for managing adipose tissue via NIR photothermal therapy. Fluorescence microscopy revealed elevated AhR expression and reduced cellular proliferation (EDU) in adipose tissue treated with PPy-based suspension microparticles w NIR, suggesting a dual mechanism of involved cellular protein level interactions and inhibited fat cell viability. The formulation's tunable characteristics (size, zeta potential, PDI) offer adaptability for biomedical applications. Future work should explore long-term efficacy, AhR-related molecular mechanisms, and broader therapeutic potential including cancer and regenerative applications by optimizing microparticle properties and NIR parameters for safe, effective, and targeted treatments. While this study demonstrates promising outcomes, several aspects warrant further assessment to strengthen translational relevance. This study used ICR mice to establish local photothermal efficacy. Future studies will include more real conditioned models and incorporate metabolic readouts to confirm efficacy and safety across clinically relevant phenotypes. Addressing these aspects in future studies can further enhance the robustness and clinical applicability of this work.

CRediT authorship contribution statement

Sih-Chi Chuang: Writing – review & editing, Writing – original draft, Methodology, Formal analysis, Data curation. **Shih-An Yu:** Writing – review & editing, Writing – original draft, Methodology, Data curation, Conceptualization. **Pei-Chia Hung:** Writing – review & editing, Writing – original draft, Methodology, Formal analysis, Data curation. **Cheng-Yi Hsiao:** Writing – review & editing, Writing – original draft, Methodology, Formal analysis, Data curation. **Lekshmi Rethi:** Writing – review & editing, Writing – original draft. **Hsu-Wei Fang:**

Writing – review & editing, Writing – original draft. **Hieu Trung Nguyen:** Writing – review & editing, Writing – original draft. **Ke Hung Tsui:** Writing – review & editing, Writing – original draft, Visualization, Validation, Supervision, Resources, Project administration, Methodology, Investigation, Funding acquisition, Formal analysis, Data curation, Conceptualization. **Andrew E.-Y. Chuang:** Writing – review & editing, Writing – original draft, Visualization, Validation, Project administration, Investigation, Funding acquisition, Formal analysis, Data curation, Conceptualization.

Consent for publication

All of the authors involved in this study have agreed to the publication of this manuscript.

Ethics approval and consent to participate

The study doesn't involve any human experiments.

Funding

This study was financially supported by grants from the National Science and Technology Council (NSTC), Taiwan [grant numbers 112-2221-E-038 -002 -MY3, 113-2314-B-038-133-MY3 and 114-2628-E-038 -001 -MY3], Taipei Medical University Hospital [grant numbers 114TMU-TMUH-02-4].

Declaration of competing interest

Given his role as Handling Editor, Andrew E.-Y. Chuang had no involvement in the peer review of this article and had no access to information regarding its peer review. Full responsibility for the editorial process for this article was delegated to another journal editor.

The authors declare that they have no known competing financial interests or personal relationships that could have appeared to influence the work reported in this paper.

Acknowledgments

This study was financially supported by grants from the National Science and Technology Council (NSTC), Taiwan [grant numbers 112-2221-E-038 -002 -MY3, 113-2314-B-038-133-MY3 and 114-2628-E-038 -001 -MY3], Taipei Medical University Hospital [grant numbers 114TMU-TMUH-02-4].

Appendix A. Supplementary data

Supplementary data to this article can be found online at https://doi.org/10.1016/j.ijbiomac.2026.150096.

Data availability

The datasets generated and/or analyzed during the current study are available from the corresponding author upon reasonable request.

References

[1] P.A. Newport-Ratiu, K.A. Hussein, T. Carter, S. Panjarian, S.C. Jonnalagadda, M. K. Pandey, Unveiling the intricate dance: obesity and TNBC connection examined, Life Sci. 357 (2024) 123082.
[2] T. Novinbahador, S. Abroon, K. Motlagh, K. Abbasi, A. Mehdizadeh, H.R. Nejabati, M. Yousefi, Surface markers on microparticles involved in obesity-derived diseases, Life Sci. 352 (2024) 122876.
[3] D.G. de Melo, V.C. da Cruz Rodrigues, G.J. de Sá Pereira, T.D.P. de Campos, R. Dos Santos Canciglieri, J.R. Pauli, A.S.R. da Silva, C.J. da Costa Fernandes, L.P. de Moura, Effects of aerobic exercise on the regulation of mitochondrial carrier homolog-2 and its influence on the catabolic and anabolic activity of lipids in the mesenteric adipose tissue of obese mice, Life Sci. 345 (2024) 122567.
[4] C. Maneechote, S.C. Chattipakorn, N. Chattipakorn, Future perspectives on the roles of mitochondrial dynamics in the heart in obesity and aging, Life Sci. 344 (2024) 122575.
[5] W. Tang, S. Wu, Y. Tang, J. Ma, Y. Ao, L. Liu, K. Wei, Microarray analysis identifies lncFirre as a potential regulator of obesity-related acute lung injury, Life Sci. 340 (2024) 122459.
[6] N.A. Patel, A. Lui, A.N. Trujillo, Z.Y. Motawe, D. Bader, J. Schuster, A. Burgess, N. G. Alves, M. Jo, J.W. Breslin, Female and male obese Zucker rats display differential inflammatory mediator and long non-coding RNA profiles, Life Sci. 335 (2023) 122285.
[7] C. Ji, X.J.N.R.E. Guo, The clinical potential of circulating microRNAs in obesity 15 (12) (2019) 731–743.
[8] E.D. Rosen, B.M.J.C. Spiegelman, What we talk about when we talk about fat 156 (1) (2014) 20–44.
[9] L. Scheja, J.J.N.R.E. Heeren, The endocrine function of adipose tissues in health and cardiometabolic disease 15 (9) (2019) 507–524.
[10] G. Barbatelli, I. Murano, L. Madsen, Q. Hao, M. Jimenez, K. Kristiansen, J. P. Giacobino, R. De Matteis, S. Cinti, The emergence of cold-induced brown adipocytes in mouse white fat depots is determined predominantly by white to brown adipocyte transdifferentiation, Am. J. Physiol. Endocrinol. Metab. 298 (6) (2010 Jun) E1244–E1253, https://doi.org/10.1152/ajpendo.00600.2009 (Epub 2010 Mar 30. PMID: 20354155).
[11] M. Harms, P.J.N.M. Seale, Brown and beige fat: development, function and therapeutic potential 19 (10) (2013) 1252–1263.
[12] J. Wu, P. Boström, L.M. Sparks, L. Ye, J.H. Choi, A.-H. Giang, M. Khandekar, K. A. Virtanen, P. Nuutila, G.J.C. Schaart, Beige adipocytes are a distinct type of thermogenic fat cell in mouse and human 150 (2) (2012) 366–376.
[13] W.D. van Marken Lichtenbelt, J.W. Vanhommerig, N.M. Smulders, J.M. Drossaerts, G.J. Kemerink, N.D. Bouvy, P. Schrauwen, G.J. Teule, Cold-activated brown adipose tissue in healthy men, N. Engl. J. Med. 360 (15) (2009 Apr 9) 1500–1508, https://doi.org/10.1056/NEJMoa0808718 (Erratum in: N Engl J Med. 2009 Apr 30;360(18):1917. PMID: 19357405).
[14] J. Nedergaard, T. Bengtsson, B. Cannon, Unexpected evidence for active brown adipose tissue in adult humans, Am. J. Physiol. Endocrinol. Metab. 293 (2) (2007 Aug) E444–E452, https://doi.org/10.1152/ajpendo.00691.2006 (Epub 2007 May 1. PMID: 17473055).
[15] K.A. Virtanen, M.E. Lidell, J. Orava, M. Heglind, R. Westergren, T. Niemi, M. Taittonen, J. Laine, N.J. Savisto, S. Enerbäck, P. Nuutila, Functional brown adipose tissue in healthy adults, N. Engl. J. Med. 360 (15) (2009 Apr 9) 1518–1525, https://doi.org/10.1056/NEJMoa0808949 (Erratum in: N Engl J Med. 2009 Sep 10;361(11):1123. PMID: 19357407).
[16] A. Vitali, I. Murano, M.C. Zingaretti, A. Frontini, D. Ricquier, S. Cinti, The adipose organ of obesity-prone C57BL/6J mice is composed of mixed white and brown adipocytes, J. Lipid Res. 53 (4) (2012 Apr) 29–619, https://doi.org/10.1194/jlr.M018846 (Epub 2012 Jan 23. PMID: 22271685; PMCID: PMC3307639).
[17] S.V. Bhadada, B.M. Patel, A.A. Mehta, R.K. Goyal, β(3) receptors: role in Cardiometabolic disorders, Ther. Adv. Endocrinol. Metab. 2 (2) (2011 Apr) 65–79, https://doi.org/10.1177/2042018810390259 (PMID: 23148172; PMCID: PMC3474626).
[18] T.M. Larsen, S. Toubro, M.A. van Baak, K.M. Gottesdiener, P. Larson, W.H. Saris, A. Astrup, Effect of a 28-d treatment with L-796568, a novel beta(3)-adrenergic receptor agonist, on energy expenditure and body composition in obese men, Am. J. Clin. Nutr. 76 (4) (2002 Oct) 780–788, https://doi.org/10.1093/ajcn/76.4.780 (PMID: 12324291).
[19] L.M. Redman, L. de Jonge, X. Fang, B. Gamlin, D. Recker, F.L. Greenway, S. R. Smith, E. Ravussin, Lack of an effect of a novel beta3-adrenoceptor agonist, TAK-677, on energy metabolism in obese individuals: a double-blind, placebo-controlled randomized study, J. Clin. Endocrinol. Metab. 92 (2) (2007 Feb) 527–531, https://doi.org/10.1210/jc.2006-1740 (Epub 2006 Nov 21. PMID: 17118998).
[20] J. Vasconcelos, E. Freire, R. Almendra, G.L. Silva, P.J.E.p. Santana, The impact of winter cold weather on acute myocardial infarctions in Portugal 183 (2013) 14–18.
[21] Z. Huang, Y. Ma, C. Li, Kappa-carrageenan inhibited the high-fat-diet-induced obesity through up-regulating the hepatic Sirt1 gene expression, Curr. Dev. Nutr. 5 (Suppl. 2) (2021 Jun 7) 503, https://doi.org/10.1093/cdn/nzab041_018.eCollection 2021 Jun.
[22] S.-C. Chuang, S.-A. Yu, P.-C. Hung, A.E.Y. Chuang, J.-W. Liang, L. Rethi, C.-K. Chen, H.-W. Fang, H.T. Nguyen, H.-T. Lu, Transformative lactera-polypyrrole@carrageenan microparticles leveraging NIR for skin regeneration and stress relief, Int. J. Biol. Macromol. 316 (2025) 144436.
[23] S.-C. Chuang, S.-A. Yu, P.-C. Hung, A.E.Y. Chuang, J.-W. Liang, C.-L. Sun, L. Rethi, H.-W. Fang, H.T. Nguyen, Y.-T. Tsai, P.-W. Weng, Mitochondrial activation via calcium peroxide/carrageenan/soybean lecithin-derived polypyrrole phototherapeutic microparticles, Colloids Surf. B: Biointerfaces 254 (2025) 114787.
[24] G. List, Soybean lecithin: food, industrial uses, and other applications, Polar lipids (2015) 1–33.
[25] D.J. Canty, S.H. Zeisel, Lecithin and choline in human health and disease, Nutr. Rev. 52 (10) (1994) 327–339.
[26] A. Joshi, S.G. Paratkar, B.N. Thorat, Modification of lecithin by physical, chemical and enzymatic methods, Eur. J. Lipid Sci. Technol. 108 (4) (2006) 363–373.
[27] S.-H. Wu, H.-T. Lu, H.T. Nguyen, P.-Y. Lin, W.-Y. Pan, A.E.Y. Chuang, Microwave-orchestrated phototherapeutic polypyrrole/soy extraction micro-complex for burn wound healing in a rodent model, J. Drug Delivery Sci. Technol. 108 (2025) 106911.

[28] C.-K. Chen, A.E.-Y. Chuang, Nanoparticles formation through photopolymerization of pyrrole with lecithin for enhanced mitochondrial activation via NIR-photothermal mild-hyperthermia, J. Polym. Res. 31 (11) (2024) 336.
[29] K.-Y. Lu, P.-R. Jheng, L.-S. Lu, L. Rethi, F.-L. Mi, E.-Y. Chuang, Enhanced anticancer effect of ROS-boosted photothermal therapy by using fucoidan-coated polypyrrole nanoparticles, Int. J. Biol. Macromol. 166 (2021) 98–107.
[30] L.E. Theune, J. Buchmann, S. Wedepohl, M. Molina, J. Laufer, M. Calderón, NIR- and thermo-responsive semi-interpenetrated polypyrrole nanogels for imaging guided combinational photothermal and chemotherapy, J. Control. Release 311 (2019) 147–161.
[31] X.-H. Wang, X.-Q. Chen, H.-S. Peng, X.-F. Wei, X.-J. Wang, K. Cheng, Y.-A. Liu, W. Yang, Facile synthesis of polypyrrole–rhodamine B nanoparticles for self-monitored photothermal therapy of cancer cells, J. Mater. Chem. B 8 (5) (2020) 1033–1039.
[32] C. Chen, J. Wang, M. Sun, J. Li, H.D. Wang, Toward the next-generation phyto-nanomedicines: cell-derived nanovesicles (CDNs) for natural product delivery, Biomed. Pharmacother. 145 (2022) 112416.
[33] Y. Zhang, M. Luo, Y. Jia, T. Gao, L. Deng, T. Gong, Z. Zhang, X. Cao, Y. Fu, Adipocyte-targeted delivery of rosiglitazone with localized photothermal therapy for the treatment of diet-induced obesity in mice, Acta Biomater. 181 (2024) 317–332.
[34] Z. Gao, Y. Liu, W. Lin, H. Lian, Z. Meng, A microneedle patch realizes weight loss through photothermal induction of fat browning, Biomater. Sci. 12 (7) (2024) 1726–1737.
[35] L. Zheng, A. Than, P. Zan, D. Li, Z. Zhang, M.K.S. Leow, P. Chen, Mild-photothermal and nanocatalytic therapy for obesity and associated diseases, Theranostics 14 (14) (2024) 5608–5620.
[36] V.E. Brunt, T.M. Eymann, M.A. Francisco, M.J. Howard, C.T. Minson, Passive heat therapy improves cutaneous microvascular function in sedentary humans via improved nitric oxide-dependent dilation, J. Appl. Physiol. (1985) 121 (3) (2016 Sep 1) 23–716, https://doi.org/10.1152/japplphysiol.00424.2016 (Epub 2016 Jul 14. PMID: 27418688; PMCID: PMC6195670).
[37] T. Laukkanen, H. Khan, F. Zaccardi, J.A. Laukkanen, Association between sauna bathing and fatal cardiovascular and all-cause mortality events, JAMA Intern. Med. 175 (4) (2015 Apr) 542–548, https://doi.org/10.1001/jamainternmed.2014.8187 (PMID: 25705824).
[38] P.L. Hooper, Hot-tub therapy for type 2 diabetes mellitus, N. Engl. J. Med. 341 (12) (1999) 924–925.
[39] A.E. Archer, R.S. Rogers, A.T. Von Schulze, J.L. Wheatley, E.M. Morris, C. S. McCoin, J.P. Thyfault, P.C. Geiger, Heat shock protein 72 regulates hepatic lipid accumulation, Am. J. Physiol. Regul. Integr. Comp. Physiol. 315 (4) (2018 Oct 1) R696–R707, https://doi.org/10.1152/ajpregu.00073.2018 (Epub 2018 Jun 20. PMID: 29924632; PMCID: PMC6230886).
[40] Y. Masuda, S. Marui, I. Kato, M. Fujiki, M. Nakada, K. Nagashima, Thermal and cardiovascular responses and thermal sensation during hot-water bathing and the influence of room temperature, J. Therm. Biol. 82 (2019 May) 83–89, https://doi.org/10.1016/j.jtherbio.2019.03.014 (Epub 2019 Mar 26. PMID: 31128663).
[41] J. Chung, A.K. Nguyen, D.C. Henstridge, A.G. Holmes, M.H. Chan, J.L. Mesa, G. I. Lancaster, R.J. Southgate, C.R. Bruce, S.J. Duffy, I. Horvath, R. Mestril, M. J. Watt, P.L. Hooper, B.A. Kingwell, L. Vigh, A. Hevener, M.A. Febbraio, HSP72 protects against obesity-induced insulin resistance, Proc Natl Acad Sci U S A 105 (5) (2008 Feb 5) 44–1739, https://doi.org/10.1073/pnas.0705799105 (Epub 2008 Jan 25. PMID: 18223156; PMCID: PMC2234214.J. Chung, A.-K. Nguyen, D.C. Henstridge, A.G. Holmes, M.S. Chan, J.L. Mesa, G.I. Lancaster, R.J. Southgate, C.R. Bruce, S.J.J.P.o.t.N.A.o.S. Duffy, HSP72 protects against obesity-induced insulin resistance 105 (5) (2008) 1739–1744).
[42] Y. Li, D. Wang, X. Ping, Y. Zhang, T. Zhang, L. Wang, L. Jin, W. Zhao, M. Guo, F. Shen, M. Meng, X. Chen, Y. Zheng, J.Q. Wang, D. Li, Q. Zhang, C. Hu, L. Xu, X. Ma, Local hyperthermia therapy induces browning of white fat and treats obesity, Cell 185 (2022).
[43] K.J. Sankaran, S. Kunuku, B. Sundaravel, P.-Y. Hsieh, H.-C. Chen, K.-C. Leou, N.-H. Tai, I.-N.J.N. Lin, Gold nanoparticle–ultrananocrystalline diamond hybrid structured materials for high-performance optoelectronic device applications 7 (10) (2015) 4377–4385.
[44] M. Stratakis, H.J.C.R. Garcia, Catalysis by supported gold nanoparticles: beyond aerobic oxidative processes 112 (8) (2012) 4469–4506.
[45] X. Zhai, P. Lei, P. Zhang, Z. Wang, S. Song, X. Xu, X. Liu, J. Feng, H.J.B. Zhang, Growth of lanthanide-doped LiGdF4 nanoparticles induced by LiLuF4 core as tri-modal imaging bioprobes 65 (2015) 115–123.
[46] J.N. Anker, W.P. Hall, O. Lyandres, N.C. Shah, J. Zhao, R.P.J.N.m. Van Duyne, Biosensing with plasmonic nanosensors 7 (6) (2008) 442–453.
[47] L. Cheng, C. Wang, Z.J.N. Liu, Upconversion nanoparticles and their composite nanostructures for biomedical imaging and cancer therapy 5 (1) (2013) 23–37.
[48] L. Feng, L. Wu, X.J.A.M. Qu, New horizons for diagnostics and therapeutic applications of graphene and graphene oxide 25 (2) (2013) 168–186.
[49] D. Jaque, L.M. Maestro, B. del Rosal, P. Haro-Gonzalez, A. Benayas, J. Plaza, E. M. Rodríguez, J.G.J.n. Solé, Nanoparticles for photothermal therapies 6 (16) (2014) 9494–9530.
[50] Y.N. Konan, R. Gurny, E.J.J.o.P, P.B. Allémann, State of the art in the delivery of photosensitizers for photodynamic therapy, Biology 66 (2) (2002) 89–106.
[51] N. Nombona, K. Maduray, E. Antunes, A. Karsten, T.J.J.o.P, P.B. Nyokong, Synthesis of phthalocyanine conjugates with gold nanoparticles and liposomes for photodynamic therapy, Biology 107 (2012) 35–44.
[52] X. Huang, I.H. El-Sayed, W. Qian, M.A. El-Sayed, Cancer cell imaging and photothermal therapy in the near-infrared region by using gold nanorods, J. Am. Chem. Soc. 128 (6) (2006 Feb 15) 2115–2120, https://doi.org/10.1021/ja057254a (PMID: 16464114).
[53] K. Haume, S. Rosa, S. Grellet, M.A. Śmiałek, K.T. Butterworth, A.V. Solov'yov, K. M. Prise, J. Golding, N.J.J.C.n. Mason, Gold nanoparticles for cancer radiotherapy: a review 7 (2016) 1–20.
[55] C.-K. Chen, S.-H. Wu, H.-T. Lu, H.T. Nguyen, P.-Y. Lin, W.-Y. Pan, K.-H. Tsui, A.E. Y. Chuang, Adipose-precise delivery of microwave-derived soybean lecithin-polypyrrole nano-pufferfish-shaped nanoparticle for localized NIR-photothermal therapy in managing obesity, Biomater. Adv. 179 (2026) 214508.
[56] W. Franco, A. Kothare, S.J. Ronan, R.C. Grekin, T.H. McCalmont, Hyperthermic injury to adipocyte cells by selective heating of subcutaneous fat with a novel radiofrequency device: feasibility studies, Lasers Surg. Med. 42 (5) (2010) 361–370.
[57] M. Purschke, H.-J. Laubach, R. Rox Anderson, D. Manstein, Thermal injury causes DNA damage and lethality in unheated surrounding cells: active thermal bystander effect, J. Invest. Dermatol. 130 (1) (2010) 86–92.
[58] S. Rao, Y. Song, F. Peddie, A. Evans, Particle size reduction to the nanometer range: a promising approach to improve buccal absorption of poorly water-soluble drugs, Int. J. Nanomedicine 6 (2011) 1245–1251.
[59] J. Rodriguez-Loya, M. Lerma, J.L. Gardea-Torresdey, Dynamic light scattering and its application to control nanoparticle aggregation in colloidal systems: a review, Micromachines (Basel) 15 (1) (2023).
[60] T. Schreiner, A. Santamaria-Echart, A. Ribeiro, A. Peres, M. Dias, S. Pinho, M. Barreiro, Formulation and optimization of nanoemulsions using the natural surfactant saponin from quillaja bark, Molecules 25 (2020) (article n° 1538).
[61] Y. Tan, K.J.S.m. Ghandi, Kinetics and mechanism of pyrrole chemical polymerization 175 (2013) 183–191.
[62] P. Kaewdee, N. Chandet, G. Rujijanagul, C.J.C.C. Randorn, Multicatalytic properties of nanoparticle CaO2 synthesized by a novel, simple and economical method for wastewater treatment 84 (2016) 151–154.
[63] R. Patil, T.J.D.D. Speaker, Carrageenan as an anionic polymer for aqueous microencapsulation 5 (3) (1998) 179–182.
[64] J. Li, M.-C. Zhao, Y.-C. Zhao, D. Yin, A. Atrens, Customization and prospects of friction stir processing for improving the biomedical properties of metallic implants for orthopedic applications, J. Mater. Res. Technol. 34 (2025) 2133–2149.
[65] M. Salehirozveh, P. Dehghani, I. Mijakovic, Synthesis, functionalization, and biomedical applications of iron oxide nanoparticles (IONPs), J. Funct. Biomater. 15 (11) (2024) 340.
[66] R.T. Oliver, H.H. Jones, D.M. Gray, B.G. Lipták, Oxidation-Reduction Potential (ORP), 2003, pp. 1506–1513.
[67] D. Polson, N. Villalba, K. Freeman, Optimization of a diagnostic platform for oxidation-reduction potential (ORP) measurement in human plasma, Redox Rep. 23 (1) (2018) 125–129.
[68] Q. Yan, B. Xin, Z. Chen, Y. Liu, Enhancement in photothermal conversion property of polypyrrole-decorated polyurethane/zirconium carbide fibrous membrane, Mater. Today Commun. 28 (2021) 102584.
[69] M. Zhang, R. Song, Y. Liu, Z. Yi, X. Meng, J. Zhang, Z. Tang, Z. Yao, Y. Liu, X. Liu, W. Bu, Calcium-overload-mediated tumor therapy by calcium peroxide nanoparticles, Chem 5 (8) (2019) 2171–2182.
[70] W.A.K. Mahmood, M.H.R. Khan, T.C. Yee, Effects of Reaction Temperature on the Synthesis and Thermal Properties of Carrageenan Ester, 2014.
[71] S. Setiadi, N. Hidayah, The effect of papain enzyme dosage on the modification of egg-yolk lecithin emulsifier product through enzymatic hydrolysis reaction, Int. J. Technol. 9 (2018) 380.
[72] I. Ibrahim, S. Yunus, A. Hashim, Relative performance of isopropylamine, pyrrole and pyridine as corrosion inhibitors for carbon steels in saline water at mildly elevated temperatures, Int. J. Sci. Eng. Res. 4 (2013).
[73] S. Zhou, Z. Cui, J.P.J.A. Urban, Factors influencing the oxygen concentration gradient from the synovial surface of articular cartilage to the cartilage–bone interface: a modeling study, Rheumatism 50 (12) (2004) 3915–3924.
[74] D. Tedesco, J. Lukas, S.I.J.G. Reed, The pRb-related protein p130 is regulated by phosphorylation-dependent proteolysis via the protein–ubiquitin ligase SCFSkp2, Development 16 (22) (2002) 2946–2957.
[75] D. Pelaez, C.-Y. Charles Huang, H.S.J.S.c. Cheung, Cyclic compression maintains viability and induces chondrogenesis of human mesenchymal stem cells in fibrin gel scaffolds, Development 18 (1) (2009) 93–102.
[76] C. Isely, M.A. Hendley, K.P. Murphy, S. Kader, P. Annamalai, E. Jabbari, R. M. Gower, Development of microparticles for controlled release of resveratrol to adipose tissue and the impact of drug loading on particle morphology and drug release, Int. J. Pharm. 568 (2019) 118469.
[77] W. Zhang, H.Q. Xie, Y. Li, M. Zhou, Z. Zhou, R. Wang, M.E. Hahn, B. Zhao, The aryl hydrocarbon receptor: a predominant mediator for the toxicity of emerging dioxin-like compounds, J. Hazard. Mater. 426 (2022) 128084.
[78] C.F.A. Vogel, L.S. Van Winkle, C. Esser, T. Haarmann-Stemmann, The aryl hydrocarbon receptor as a target of environmental stressors - implications for pollution mediated stress and inflammatory responses, Redox Biol. 34 (2020) 101530.
[79] J. Yin, B. Sheng, Y. Qiu, K. Yang, W. Xiao, H. Yang, Role of AhR in positive regulation of cell proliferation and survival, Cell Prolif. 49 (5) (2016) 554–560.
[80] S.M. Ronnekleiv-Kelly, M. Nukaya, C.J. Díaz-Díaz, B.W. Megna, P.R. Carney, P. G. Geiger, G.D. Kennedy, Aryl hydrocarbon receptor-dependent apoptotic cell death induced by the flavonoid chrysin in human colorectal cancer cells, Cancer Lett. 370 (1) (2016) 91–99.
[81] J. Vondráček, K. Pěnčíková, J. Neča, M. Ciganek, A. Grycová, Z. Dvořák, M.J.E. p. Machala, Assessment of the aryl hydrocarbon receptor-mediated activities of

polycyclic aromatic hydrocarbons in a human cell-based reporter gene assay 220 (2017) 307–316.
[82] Y.-C. Liang, Y.-S. Cheng, H.-Y. Chen, H.-M.D. Wang, Bio-hydrogel from RGD peptide/chitosan/β-glycerophosphate prevents postoperative wound adhesion, Int. J. Biol. Macromol. 284 (2025) 137938.
[83] S. Cheng, J. Li, Y.-Q. Song, S. Jing, Y.-X. Lan, L. Wang, D.S.-H. Chan, C.-Y. Wong, C. Sheng, W. Wang, H.-M.D. Wang, C.-H. Leung, A bioactive benzimidazole-cyclometalated iridium(III) complex as an epigenetic regulator through effectively interrupting the EED–EZH2 interaction, Small 21 (12) (2025) 2405771.
[84] H. Ning, M. Albersen, G. Lin, T.F. Lue, C.S. Lin, Effects of EdU labeling on mesenchymal stem cells, Cytotherapy 15 (1) (2013) 57–63.
[86] K.C. Yoon, K.G. Kim, NIR irradiation based on low-power LED drive module design for fat reduction, Biomed. Res. Int. 2021 (2021) 9992095.
[87] Y. Li, D. Wang, X. Ping, Y. Zhang, T. Zhang, L. Wang, L. Jin, W. Zhao, M. Guo, F. Shen, M. Meng, X. Chen, Y. Zheng, J. Wang, D. Li, Q. Zhang, C. Hu, L. Xu, X. Ma, Local hyperthermia therapy induces browning of white fat and treats obesity, Cell 185 (6) (2022) 949–966.e19.
[88] I. Yanina, N. Navolokin, A. Bucharskaya, G. Maslyakova, V. Tuchin, Skin and subcutaneous fat morphology alterations under the LED or laser treatment in rats in vivo, J. Biophotonics 12 (2019).
[89] F. Li, T.S.Y. Choong, S. Soltani, L.C. Abdullah, S.N.A. Md, N.N.A. Nuar, Investigation of glyphosate removal from aqueous solutions usingFenton-like system based on calcium peroxide, Processes 10 (2045) (2022) 2022.